Supporting Information

Gas-Phase Synthesis of Germanium Monosulfide (GeS, $X^1\Sigma^+$) via the Elementary Reaction of Atomic Germanium (Ge, ^3P) with Hydrogen Sulfide (H_2S, X^1A_1)

Surajit Metya,[a] Shane J. Goettl,[a] Iakov A. Medvedkov,[a] Márcio O. Alves[b], Breno R. L. Galvão,*[b]
Ralf I. Kaiser*[a]

a Department of Chemistry, University of Hawai'i at Manoa, Honolulu, HI 96822, USA.
E-mail: ralfk@hawaii.edu
b Centro Federal de Educação Tecnológica de Minas Gerais, Belo Horizonte 30421-169, Brazil.
E-mail: brenogalvao@gmail.com

Keywords: crossed molecular beams, intersystem crossing, reaction dynamics, germanium, GeS, germanium monosulfide

Content

Note S1: **Crossed molecular beam experiment**

The crossed molecular beam experiment is a powerful technique for investigating reaction products, intermediates, and branching ratios in bimolecular reactions.[1-5] Its primary advantage lies in enabling the study of reactions resulting from bimolecular collisions with precisely defined velocity, angular distribution, and internal quantum states. Unlike bulk experiments, the crossed molecular beam technique confines the colliding species into separate beams that intersect at a specific angle. Each of the beams is highly diluted, minimizing collisions within the beam itself. These characteristics provide a distinctive method for studying reactions from a single molecular collision while preventing secondary collisions and wall interactions.

In our crossed molecular beam experiment two stationary supersonic molecular beam sources, generated from the adiabatic expansion of the high-pressure gas into the evacuated chambers, are crossing each other at 90°. The adiabatic expansion leads the random thermal motion in the high-pressure zone into a forward directed flow of a cold molecular beam. Detailed of the instrumental set-up is described elsewhere.[4-6] Detection of the scattering products is achieved through Time-of-Flight (TOF) mass spectrometry using a rotatable universal detector which consist of Brink-type electron impact ionizer, quadrupole mass filter and the Daly-type scintillation particle detector. In this TOF recoding process, mass controller is fixed at specific mass to change ratio (*m/z*) and measure the time-dependent number density of the reactively scattered species at this *m/z* and a fixed angle Θ, $I(\Theta, t)$. Laboratory (LAB) angular distribution of the reactively scattered product is determined by integrating the intensity of the recoded TOF spectra at different laboratory angles.

To achieve a detailed physical understanding of the reaction mechanism, including the assignment of intermediates and identification of reaction products, it is essential to transform the laboratory (LAB) angular distributions and TOF spectra into the center-of-mass (CM) frame using a forward-convolution method. Theoretical details for this transformation are provide in the reference [6]. In general, this process initially assumes trial angular, $T(\theta)$ and translation energy, $P(E_T)$ distribution in the center of mass (CM) reference frame. TOF spectra and LAB angular distribution are then calculated from these $T(\theta)$ and $P(E_T)$ averaging over the instrument and beam functions. This process is repeated until a satisfying fit of the laboratory data is achieved. The final output of the experiments is a product flux contour map, which presents the differential cross section, i.e., the intensity of the reactively scattered products, expressed as $I(\theta,u) \sim P(u) \times T(\theta)$, where the intensity is mapped as a function of the scattering angle θ and the product center-of-mass velocity u. These contour plots of a bimolecular reactive scattering process serve multiple purposes: (i) identifying the primary reaction products, (ii) determining the branching ratios, (iii) elucidating the microscopic reaction mechanism, (iv) estimating the product energy release, and (v) providing insights into the potential energy surface (PES). To understand the reaction energetics, we must closely examine the center-of-mass velocity u of the products, as it directly relates to their translational energy. The chemical reaction dynamics can be explored by analyzing three key features of the product flux distribution $I(\theta,u)$. First, when the energetics of product isomers are well separated, the maximum translational energy ($E_{\max}$) can help identify the nature of the products. $E_{\max}$ is the sum of the reaction exoergicity, obtained from electronic structure calculations or literature, and the collision energy (Ec) used in the experiment. By subtracting the collision energy from the experimentally determined $E_{\max}$, one can directly estimate the reaction exoergicity. Second, the peak position of the translational energy distribution $P(E_T)$ can, in favorable cases, provide an estimate of the exit barrier height. If $P(E_T)$ peaks near zero, it suggests a barrierless or low-barrier bond rupture, indicating a loose exit transition state. In contrast, if $P(E_T)$ exhibits a pronounced maximum at higher translational energies, this implies a tight transition state with significant changes in geometry and electron density during product formation. Third, analyzing the fraction of total energy released into translational motion offers insight into the reaction mechanism. A translational energy fraction of about 30–40% typically indicates the formation of a long-lived, covalently bound intermediate. In contrast, a significantly higher fraction is characteristic of direct, non-complex-forming reaction dynamics.

The angular component of the flux contour maps provides the function $T(\theta)$, which is critical for understanding chemical reaction dynamics and identifying the intermediates involved. These plots represent the angular distribution of the flux as observed from a reference frame moving with the center-of-mass (CM) of the reacting system. In this frame, the direction of the primary beam is defined as 0°, and that of the secondary beam as 180°. Several distinct shapes of the flux distribution $I(\theta,u)$ can emerge, each offering different insights into the reaction mechanism:

1. Forward-Backward Symmetric Distributions: If $T(\theta)$ and the corresponding $I(\theta,u)$ show symmetry around 90°, it indicates forward-backward symmetry. This behavior is typical of bimolecular reactions like $A + BC \rightarrow AB + C$, proceeding via a long-lived $[ABC]^*$ intermediate, indicative of indirect scattering dynamics. Here, the intermediate survives longer than its rotational

period, allowing it to rotate multiple times and lose memory of the reactant approach direction. In this case, the flux distribution appears symmetric, but the precise shape of T(θ) is governed by the distribution of total angular momentum, influenced by correlations between initial and final angular momentum and the final rotational state of the products.

2. Asymmetric Distributions: An asymmetric angular distribution around 90°, often with stronger flux at 0° than at 180°, may suggest an "osculating complex" model. In such cases, the reaction still proceeds via an intermediate, but its lifetime is comparable to its rotational period—allowing only limited rotation before dissociation. Alternatively, the asymmetry may arise from two reaction pathways or microchannels: one producing a symmetric flux and the other favoring forward scattering. Monitoring how T(θ) changes with increasing collision energy helps differentiate between these scenarios. A shift from symmetric to forward-scattered distributions support the osculating complex model, whereas reduced forward peaking with increased energy supports the two-channel interpretation.

3. Strongly Directional Distributions: In some cases, the angular flux distribution peaks sharply in one direction, either at 0° ("stripping dynamics") or at 180° ("rebound dynamics"), with minimal flux at other angles. These profiles are characteristic of “direct” reaction dynamics, where the reaction either bypasses an intermediate entirely or involves a highly excited, extremely short-lived intermediate (lifetime less than 0.1 picoseconds). Such mechanisms are typically associated with repulsive or weakly attractive potential energy surfaces, as opposed to the deep potential wells seen in indirect dynamics involving long-lived intermediates.

Table S1. Experimentally determined peak velocities (Vp) and speed ratios (S) of the germanium (Ge), and hydrogen sulfide (H_2S) beams along with the corresponding collision energies (E_C) and center-of-mass angles (Θ_{CM})

Beam	V_p (m s^{-1})	S	E_c kJ mol^{-1}	Θ_{CM} (°)
Ge (^3P)	2683 ± 26	2.5 ± 0.2		
H_2S (X^1A_1)	805 ± 9	12.4 ± 0.1	91 ± 2	8.25

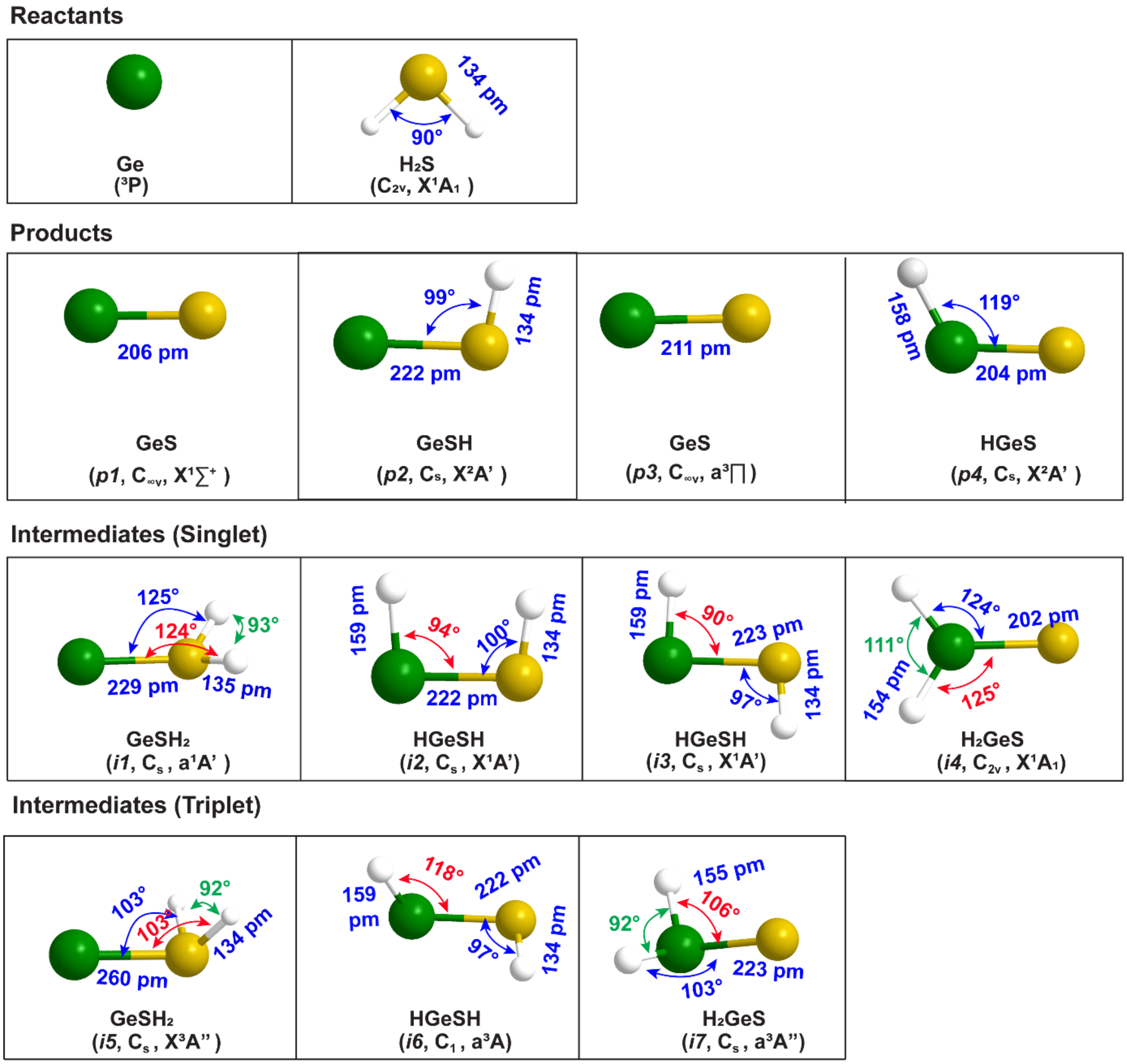

Figure S1. Optimized geometries of the reactants, products, and intermediates for the reaction of ground state germanium atom (Ge, ^{3}P) and hydrogen sulfide (H_2S, X^1A_1) calculated at M06-2X/cc-pVTZ level of theory. Atoms are color coded in green (germanium), yellow (sulfur), and white (hydrogen).

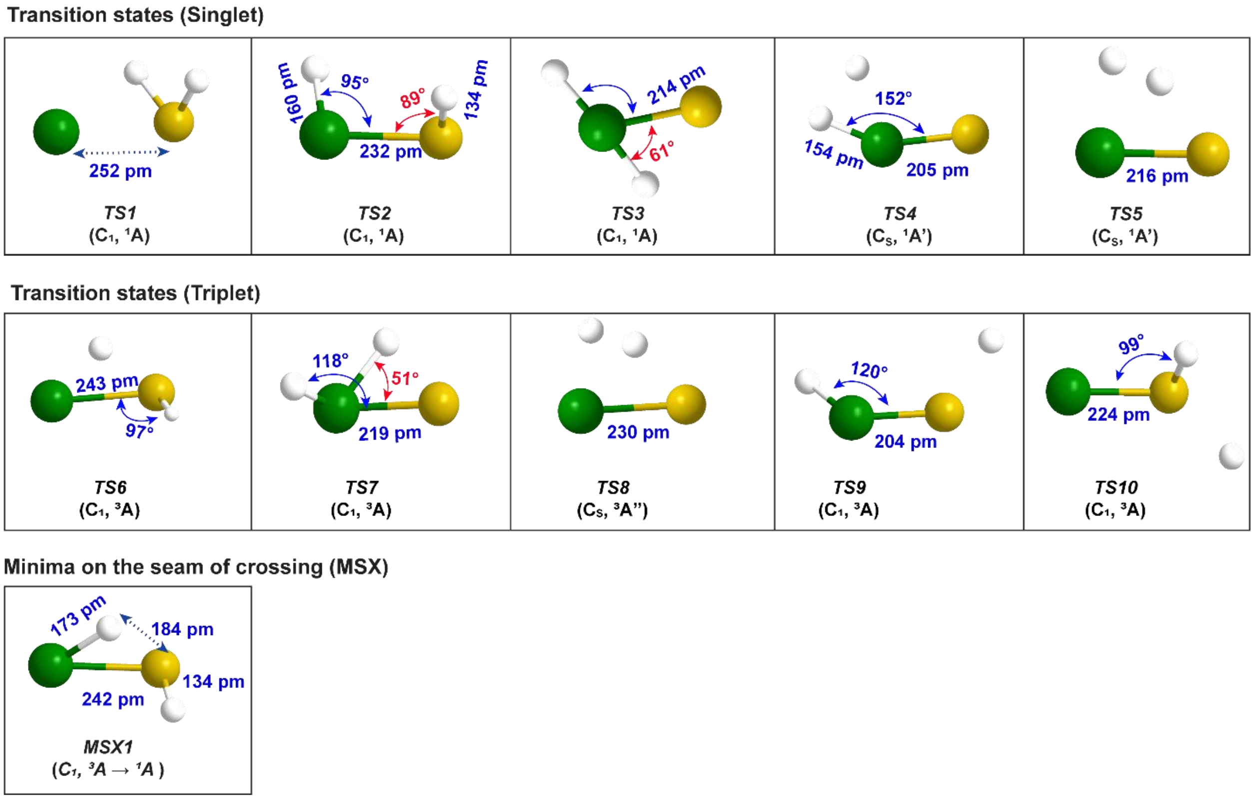

Figure S2. Optimized geometries of the singlet and triplet transition states, and the minimum of the seam of crossing (MSX) for the reaction of ground state germanium atom (Ge, ^3P) and hydrogen sulfide (H_2S, X^1A_1) calculated at M06-2X/cc-pVTZ level of theory. Atoms are color coded in green (germanium), yellow (sulfur), and white (hydrogen).

Note S2: **Calculation of energy-dependent rate constat**

The energy-dependent RRKM (Rice−Ramsperger−Kassel−Marcus)[7] rate constants are estimated for the unimolecular reaction steps on the singlet surface at collision energies of 0.0 and 91 ± 2 kJ mol^{-1}. This computation utilizes the relative energies, and the molecular parameters obtained from the electronic structure calculation. The internal energy of each $GeSH_2$ species was considered as the sum of the collision energy and the chemical activation energy, where the latter is defined as the negative of the relative energy of the specific structure on the potential energy surface (PES) with respect to the separated reactants. The energy-dependent rate constants were calculated using our in-house code under zero-pressure conditions, simulating both crossed molecular beam experiments and outer space environments. Finally, the RRKM-derived rate constants were employed to determine the product branching ratios under the steady-state approximation.[8, 9]

Table S2. The RRKM rate constants (s^{-1}) computed using CCSD(T)-F12/aug-cc-pVQZ//M06-2X/cc-pVTZ + ZPE(M06-2X/cc-pVTZ) energies with M06-2X/cc-pVTZ harmonic frequencies for the molecular hydrogen loss channel of Ge + H2S reaction on the singlet surface considering the intermediate ***i2*** as the starting point.

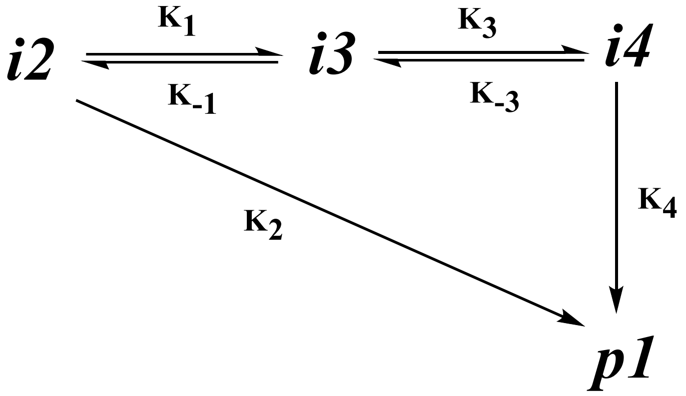

Rate constant	At 0 kJ mol^{-1}	At 91 kJ mol^{-1}
$\mathbf{k_{1}}$	6.18×10^{12}	8.67×10^{12}
$\mathbf{k_{-1}}$	6.01×10^{12}	8.77×10^{12}
$\mathbf{k_{2}}$	3.80×10^{11}	1.28×10^{12}
$\mathbf{k_{3}}$	1.60×10^{10}	4.50×10^{11}
$\mathbf{k_{-3}}$	6.04×10^{10}	1.53×10^{12}
$\mathbf{k_{4}}$	0.00×10^{0}	5.67×10^{10}

Table S3. Calculated harmonic frequencies (in cm^{-1}) of the products, intermediates and transition states for the reaction between atomic germanium (Ge, ^3P) and hydrogen sulfide (H_2S, X^1A_1) at the M06-2X/cc-pVTZ level of theory

Products				
p1	***p2***	***p3***	***p4***	H_2
602	398	452	514	4440
	679		568	
	2690		1927	

Intermediates						
i1	***i2***	***i3***	***i4***	***i5***	***i6***	***i7***
177	394	402	532	175	284	401
302	484	532	581	359	403	431
593	680	618	606	391	555	603
1326	774	866	890	1222	655	812
2491	1951	1957	2153	2706	2011	2063
2570	2743	2726	2161	2711	2700	2095

Transition States									
TS1	***TS2***	***TS3***	***TS4***	***TS5***	***TS6***	***TS7***	***TS8***	***TS9***	***TS10***
-735	-625	-1358	-1579	-1834	-461	-1141	-2083	-391	-558
171	354	372	461	487	330	445	312	141	169
486	592	507	530	927	493	546	653	219	381
1237	716	685	551	954	676	613	760	524	414
2152	1921	1839	1423	1534	1438	1644	1465	563	726
2562	2686	2019	2144	1670	2709	1998	1628	1932	2695

Table S4. Optimized Cartesian coordinates for all the reactants, products, intermediates, transition states and minima-on-the-seam-of-crossings (MSX) for the reaction between ground state germanium atom (Ge, ^3P) and hydrogen sulfide calculated at M06-2X/cc-pVTZ level of theory

Reactant							
Ge (^3P)				**H_2S (X^1A_1)**			
Ge	0.0000	0.0000	0.0000	S	-2.3471	0.9336	0.0195
				H	-1.0242	1.1287	-0.0309
				H	-2.5982	2.2064	-0.3092
Products							
p1 **(GeS, $X^1\Sigma^+$)**				***p3*** **(GeS, $a^3\Pi$)**			
Ge	-5.6878	4.9132	0.0000	Ge	-5.7293	4.9339	0.0000
S	-3.8812	4.0168	0.0000	S	-3.8396	3.9961	0.0000
p2 **(GeSH, X^2A')**				***p4*** **(*HGeS*, X^2A')**			
Ge	-5.0594	1.8277	0.0000	Ge	-5.4146	1.5189	0.0000
S	-2.9306	1.1811	0.0000	S	-3.3724	1.5507	0.0000
H	-2.3430	2.3895	0.0000	H	-6.2052	2.8837	0.0000
H_2 ($X^1\Sigma_g$)							
H	-6.9514	2.1180	0.0000				
H	-6.2248	1.9686	0.0000				
Intermediates							
i1 **($GeSH_2$, a^1A')**				***i2*** **(HGeSH, X^1A')**			
S	-0.3074	-0.0101	0.9973	S	0.0000	-0.0364	-1.0486
H	0.0575	-1.0025	1.8449	H	0.0001	1.4810	1.3435
H	0.0648	0.9730	1.8513	H	-0.0001	1.2899	-1.2333
Ge	0.0907	0.0045	-1.2589	Ge	0.0000	-0.1028	1.1935
i3 **(HGeSH, X^1A')**				***i4*** **(H_2GeS, X^1A_1)**			
S	0.0953	0.1993	-1.2707	Ge	0.0000	0.0000	0.9833
H	-1.5899	-0.0411	0.8650	H	1.2679	0.0000	1.8608
H	1.3596	0.6330	-1.3776	H	-1.2678	0.0000	1.8608
Ge	-0.0998	0.5129	0.9293	S	0.0000	-0.0001	-1.0454
i5 **($GeSH_2$, X^3A'')**				***i6*** **(HGeSH, a^3A)**			
S	0.0000	-0.0532	1.1501	S	-0.0287	-0.0308	-1.0589
H	0.9692	0.8171	1.4758	H	-1.2537	0.1103	1.9501

H	-0.9692	0.8171	1.4758
Ge	0.0000	-0.0011	-1.4455

H	0.1535	1.2840	-1.2643
Ge	0.0853	0.0083	1.1605

i7 **(H_2GeS, a ^{3}A”)**

Ge	0.0000	-0.4603	1.1444
H	1.2737	0.1773	1.7635
H	-1.2736	0.1773	1.7635
S	0.0000	0.1058	-1.0119

Transition states

TS1 **(^{1}A)**

S	0.0333	-0.0354	1.1262
H	0.7058	0.9614	0.4293
H	-0.6834	0.9858	1.6563
Ge	-0.0290	-0.0163	-1.3971

TS2 **(^{1}A)**

S	0.2910	-0.1355	-1.3434
H	-1.5012	0.6818	0.8340
H	0.7963	1.1119	-1.3719
Ge	-0.0222	0.0844	0.9411

TS3 **(^{1}A)**

Ge	0.1360	0.3733	1.0994
H	1.3797	-0.1874	0.2416
H	-1.0251	-0.2465	1.9456
S	-0.1358	0.0316	-0.9912

TS4 **(^{1}A’)**

Ge	0.0000	0.1072	0.9896
H	0.0000	-1.5962	1.5112
H	0.0000	-0.5348	2.3938
S	0.0000	-0.0186	-1.0519

TS5 **(^{1}A’)**

S	-0.0324	-0.2101	-1.1613
H	0.0317	1.7218	0.6324
H	0.0094	1.2646	-0.2912
Ge	0.0018	-0.0482	0.9916

TS6 **(^{3}A)**

S	0.0083	-0.0570	-1.1200
H	-1.0597	0.6745	0.1654
H	0.5834	1.1425	-1.3007
Ge	0.0319	-0.0174	1.3150

TS7 **(^{3}A)**

Ge	0.0797	-0.4878	1.1106
H	1.2205	0.1995	1.9277
H	-0.7959	0.7553	0.3613
S	-0.0841	-0.0173	-1.0218

TS8 **(^{3}A”)**

S	-0.0337	-0.1882	-1.2211
H	0.0276	1.6822	0.6132
H	0.0101	1.2431	-0.2970
Ge	0.0064	-0.0090	1.0764

TS9 **(^{3}A)**

S	-0.1893	0.0371	-0.9087
Ge	0.0222	-0.0936	1.1230

TS10 **(^{3}A)**

S	-0.1078	-0.0697	-0.9388
H	-0.2258	1.2405	-1.2099

H	-0.1207	1.2050	2.0044	H	1.5738	0.1585	-2.2521
H	1.9971	0.0476	-2.0302	Ge	-0.0284	0.0282	1.3007

MSX1

S	0.0136	-0.0542	-1.1150
H	-1.0731	0.6745	0.1754
H	0.5897	1.1411	-1.3079
Ge	0.0338	-0.0187	1.3073

References:

(1) Lee, Y. T. Molecular Beam Studies of Elementary Chemical Processes. *Science* **1987**, *236*, 793-798

(2) Lee, Y. T. Molecular Beam Studies of Elementary Chemical Processes (Nobel Lecture). *Angew. Chem. Int. Ed.* **1987**, *26*, 939-951

(3) Levine, R. D.; Bernstein, R. B. *Molecular Reaction Dynamics and Chemical Reactivity*; Oxford University Press, Oxford, **1987**.

(4) Kaiser, R. I.; Maksyutenko, P.; Ennis, C.; Zhang, F.; Gu, X.; Krishtal, S. P.; Mebel, A. M.; Kostko, O.; Ahmed, M. Untangling the chemical evolution of Titan's atmosphere and surface–from homogeneous to heterogeneous chemistry. *Faraday Discuss.* **2010**, *147*, 429-478

(5) Kaiser, R. I. Experimental investigation on the formation of carbon-bearing molecules in the interstellar medium via neutral− neutral reactions. *Chem. Rev.* **2002**, *102*, 1309-1358

(6) Krasnoukhov, V. S.; Azyazov, V. N.; Mebel, A. M.; Doddipatla, S.; Yang, Z.; Goettl, S.; Kaiser, R. I. Combined Crossed Molecular Beams and Ab Initio Study of the Bimolecular Reaction of Ground State Atomic Silicon (Si; 3P) with Germane (GeH4; X1A1). *ChemPhysChem* **2021**, *22*, 1497-1504

(7) Chang, A. H.; Mebel, A.; Yang, X.-M.; Lin, S.; Lee, Y. Ab initio/RRKM approach toward the understanding of ethylene photodissociation. *J. Chem. Phys.* **1998**, *109*, 2748-2761

(8) Kislov, V.; Nguyen, T.; Mebel, A.; Lin, S.; Smith, S. Photodissociation of benzene under collision-free conditions: An ab initio/Rice–Ramsperger–Kassel–Marcus study. *J. Chem. Phys.* **2004**, *120*, 7008-7017

(9) He, C.; Zhao, L.; Thomas, A. M.; Morozov, A. N.; Mebel, A. M.; Kaiser, R. I. Elucidating the chemical dynamics of the elementary reactions of the 1-propynyl radical (CH3CC; X2A1) with methylacetylene (H3CCCH; X1A1) and allene (H2CCCH2; X1A1). *J. Phys. Chem. A* **2019**, *123*, 5446-5462